

Electronic Supplementary Information (ESI)

Lab Chip, (2019), DOI: 10.1039/c9lc00071b

High-throughput electrical position detection of single flowing particles/cells with non-spherical shape[†]

Riccardo Reale,^a Adele De Ninno,^a Luca Businaro,^b

Paolo Bisegna,^a and Federica Caselli*^a

^a *Department of Civil Engineering and Computer Science, University of Rome Tor Vergata*

E-mail: caselli@ing.uniroma2.it

^b *Institute for Photonics and Nanotechnologies, Italian National Research Council*

1 Previously reported strategy for lateral position determination

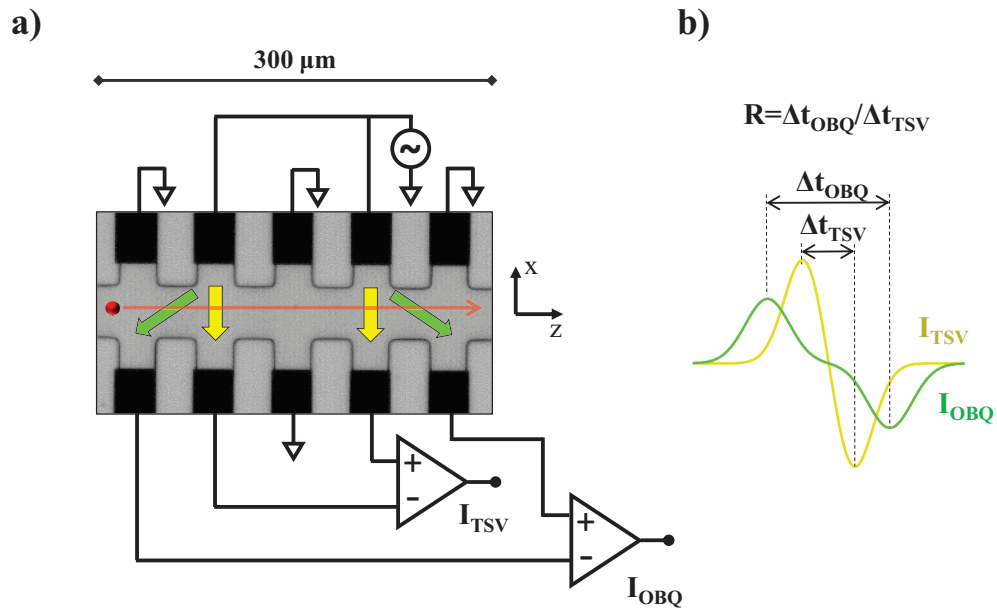


Figure S1: Strategy for lateral position determination used in Ref. [28] of the main text. (a) Five pairs of coplanar electrodes housed in lateral channels are used. An AC voltage is applied to two electrodes and two differential current signals are collected: I_{OBQ} , featuring a current path with oblique orientation (green arrows), and I_{TSV} , featuring a current path with transverse orientation (yellow arrows). (b) Each signal has a bipolar Gaussian shape. The ratio R of the peak-to-peak times of the two signals, $R = \Delta t_{OBQ} / \Delta t_{TSV}$, encodes particle lateral position (x -coordinate). In particular, it is close to one for particles traveling near the channel wall at positive x , and it increases moving away from that wall.

2 Gallery of simulated signals (spherical particle)

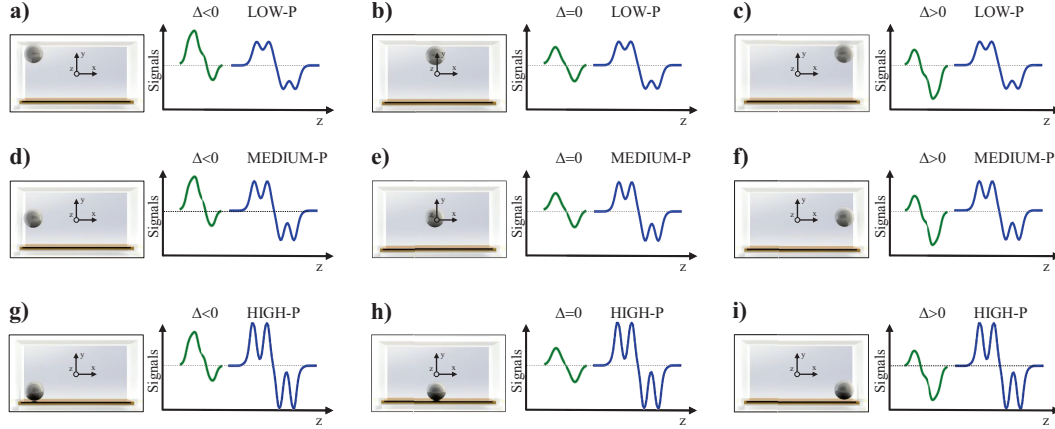


Figure S2: Differential signals I_{Δ} (green) and I_P (blue) produced by a spherical particle passing through the sensing regions at nine different cross-sectional positions (finite element simulation results, real part of the signals shown). If the particle is centered along x the amplitude relative difference Δ is 0 (b, e, h), whereas if the particle travels near the channel lateral walls it results $\Delta < 0$ (a, d, g) or $\Delta > 0$ (c, f, i) according to $x < 0$ or $x > 0$, respectively. If the particle travels near the top (a–c) [resp. bottom (g–i)] of the channel, the relative prominence P is low [resp. high]; if the particle is centered along y (d–f), an intermediate relative prominence P is found.

3 Parameter values used in the FEM simulations

Table S1: Dielectric parameters used in the FEM simulations relevant to Figure 4 of the main text, and Figures S2 and S5.

Parameter	Value
bead/prolate ellipsoid conductivity	0.67×10^{-3} S/m
erythrocyte cytoplasm conductivity	0.5 S/m
buffer conductivity	1.6 S/m
bead/prolate ellipsoid relative permittivity	2.5
erythrocyte cytoplasm relative permittivity	60
buffer relative permittivity	80
erythrocyte membrane capacitance	0.01 F/m ²
electrode double-layer capacitance	14.4 F/m ²
frequency of AC voltage	500 kHz

4 Optical estimate of lateral position

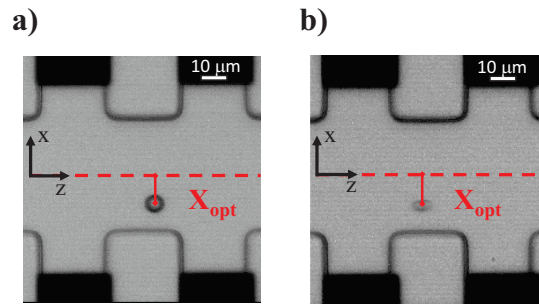


Figure S3: An optical estimate X_{opt} of particle lateral position is determined as the distance between particle center and channel z -axis. Exemplary snapshots of a flowing bead (a) or a flowing erythrocyte (b) are shown.

5 Calibration procedure

The calibration experiment C (cf. Table 1 of the main text) is considered. Accounting for finite particle diameter $d = 7 \mu\text{m}$, and allowing for small gaps between particle boundary and channel walls ($g_{\text{lat}} \sim 10\% W$ along x , $g_{\text{vert}} \sim 10\% H$ along y), particle center coordinates satisfy the following inequalities:

$$|x| \leq W/2 - s_{\text{lat}}, \quad |y| \leq H/2 - s_{\text{vert}}, \quad (1)$$

where $s_{\text{lat}} = d/2 + g_{\text{lat}}$ and $s_{\text{vert}} = d/2 + g_{\text{vert}}$. Accordingly, parameters β and γ appearing in Eq. (3) of the main text were determined by imposing the conditions:

$$X(\Delta_{\text{L}}) = -\frac{W}{2} + s_{\text{lat}}, \quad X(\Delta_{\text{H}}) = +\frac{W}{2} - s_{\text{lat}}, \quad (2)$$

where Δ_{L} and Δ_{H} are the 1% and 99% percentile values of Δ , respectively (Figure S4(a), red lines). Their values are reported in Table S2, along with the resulting calibration coefficients β and γ . It is noticed that a small value of the parameter γ was found ($\gamma = -0.02$, ascribable to a $1 \mu\text{m}$ misalignment between the electrodes and the PDMS channel).

Similarly, the parameters c_0 , c_1 , c_2 entering Eq. (4) of the main text were determined by imposing the conditions:

$$Y(P_{\text{L}}) = \frac{H}{2} - s_{\text{vert}}, \quad Y(P_{\text{H}}) = -\frac{H}{2} + s_{\text{vert}}, \quad Y(P_{\text{M}}) = 0, \quad (3)$$

where P_{L} and P_{H} are the 1% and 99% percentile values of P , respectively (Figure S4(a), green lines), and P_{M} is the relative prominence value corresponding to channel axis $y = 0$ (identified by maximum particle velocity, cf. Figure S4(b)). The values of P_{L} , P_{M} , and P_{H} are reported in Table S3, along with the resulting calibration coefficients c_0 , c_1 and c_2 .

Table S2: Values of 1% and 99% percentile of Δ , Δ_{L} and Δ_{H} , respectively, and resulting calibration parameters β , γ (Eq. (3) of the main text).

Δ_{L}	Δ_{H}	β	γ
-0.62	0.71	0.49	-0.02

Table S3: Values of 1% and 99% percentile of P , P_{L} and P_{H} , respectively, and value of P at maximum velocity, P_{M} . Resulting calibration parameters c_0 , c_1 , c_2 (Eq. (4) of the main text).

P_{L}	P_{M}	P_{H}	c_0	c_1	c_2
0.09	0.37	0.83	0.34	-1.07	0.45

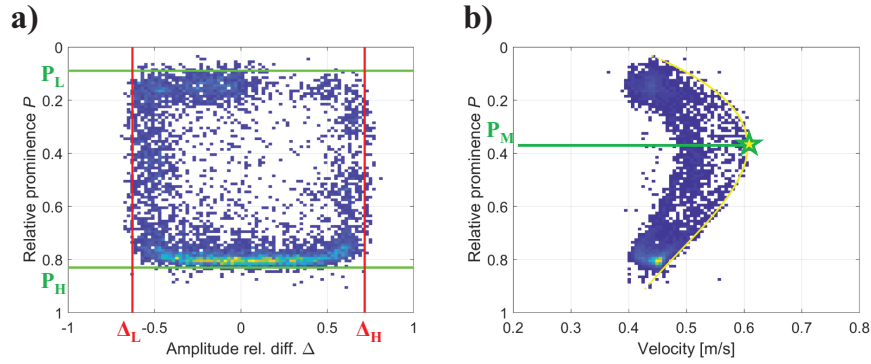


Figure S4: Calibration experiment (sample flow rate $Q_{sa} = 15 \mu\text{l}/\text{min}$, right and left sheath flow rates $Q_{sh}^R = Q_{sh}^L = 2.5 \mu\text{l}/\text{min}$). a) Density plot of relative prominence P versus amplitude relative difference Δ . The 1% and 99% percentile values of Δ (red lines) and P (green lines) are shown. The corresponding values are labelled as Δ_L , Δ_H (Table S2), and P_L , P_H (Table S3). b) Density plot of particle velocity versus relative prominence P . The cubic 95% quantile regression is shown in yellow. The relative prominence value P_M corresponding to the maximum velocity $V_{\max} = 0.6 \text{ m/s}$ is visualized (Table S3). Particle velocity was computed from the transit time of the differential signal I_P .

6 Full set of simulated RBC orientations

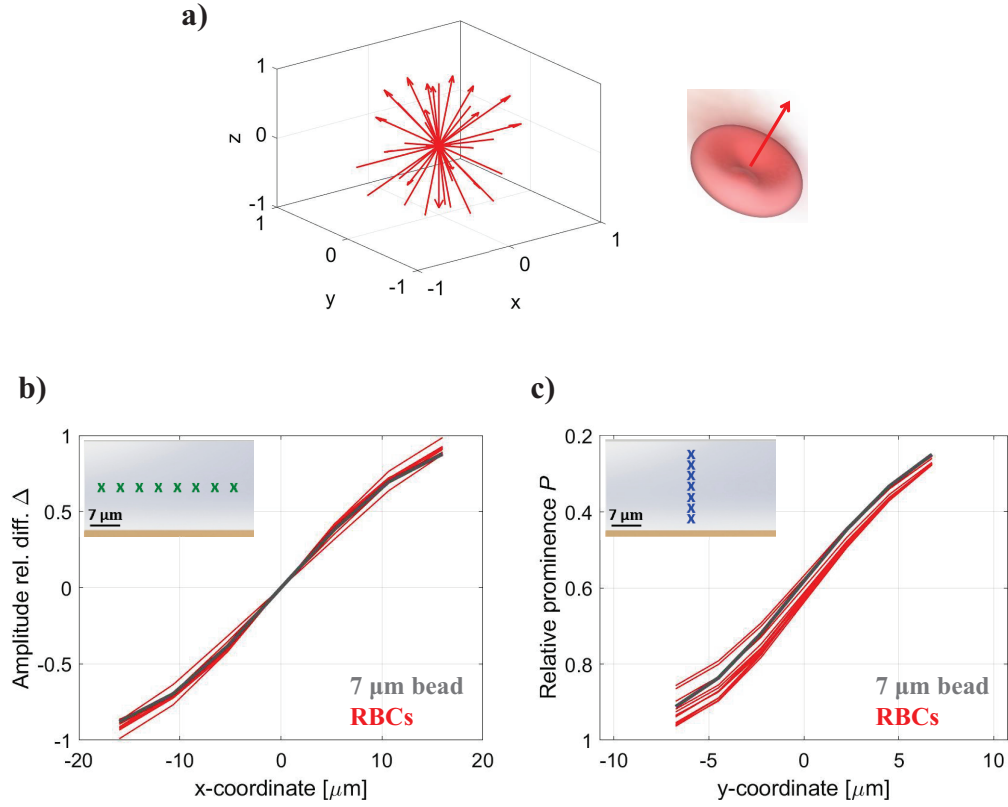


Figure S5: (a) Visualization of the different orientations of the erythrocyte axisymmetry axis used in simulations. (b) Amplitude relative difference Δ as a function of particle lateral position (x -coordinate) and (c) relative prominence P as a function of particle vertical position (y -coordinate). Different curves refer to the orientations represented in panel (a). Selected orientations (red blood cell oriented along the x -, y - or z -axis) are visualized in Figure 4(a) of the main text.

7 Chicken red blood cells

In order to further demonstrate the suitability to cells with non-spherical shape of the proposed position-detection approach, an experimental campaign involving chicken red blood cells was carried out. Whereas a (healthy) human red blood cell has the shape of a biconcave disc, a chicken red blood cell has the shape of a prolate ellipsoid. Typical dimensions are $7 \mu\text{m}$ (short diameter) and $12 \mu\text{m}$ (long diameter). Figure S6 and Figure S7 report the optical validation and a representative position-detection experiment, respectively. Channel width is $40 \mu\text{m}$, a grounded electrode is present $60 \mu\text{m}$ upstream the lateral position sensing zone, and no sheath flows are used.

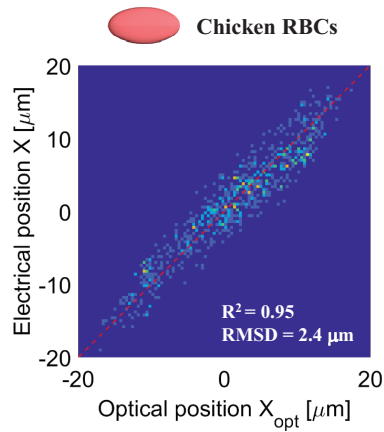


Figure S6: Comparison between optical estimate X_{opt} and electrical estimate X of lateral positions of chicken red blood cells (~ 4900 events). The bisector line is dashed in red. The regression coefficient and the root-mean-squared difference RMSD are also reported.

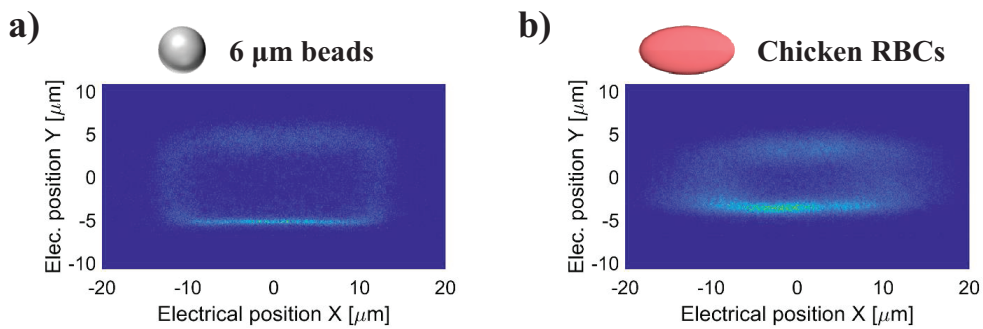


Figure S7: Density plots of the electrical cross-sectional positions (X, Y) of (a) $6 \mu\text{m}$ beads (~ 25000 events) and (b) chicken red blood cells (~ 110000 events). The flow rate is $30 \mu\text{l}/\text{min}$ and the average throughput is 460 events/s. A certain degree of inertial focusing is noticed.

8 Longitudinal position sensing by noisy impedance measurements

In a recent work (Ref. [27] of the main text), Brazey et al. proposed the application of the Extended Kalman Filter (EKF) for the real-time detection of particle longitudinal position (i.e., along channel length) based on noisy impedance measurements. The impedance variation as a function of particle longitudinal position was used as observation model, and was obtained by calibration with a camera (Figure 8 of Ref. [27]). Because the observation model must be the same for all particles (except for the noise), a dielectrophoretic (DEP) focusing module was used, in order to eliminate variability due to particle position in the channel section. As a proof of concept, those Authors presented experimental validation on a 1D case to determine the longitudinal position of $8.7 \mu\text{m}$ diameter beads from the variation of impedance measured between two electrodes. We refer the Reader to the original paper (Ref. [27], Section 4) and the references therein for a comprehensive presentation of that approach and for the theory of Kalman filtering.

In this section we report on a modified version of the approach proposed by Brazey et al., which has been implemented using our chip. Instead of a DEP module, we use sheath flows to center the particles along the channel width. Our method does not require particle centering along the channel height, because we build the observation model from the signal I_{Δ} , which is independent from particle vertical position. In particular, our observation model (Figure S8(a)) is obtained by scaling the abscissa of I_{Δ} (impedance variation as a function of time) according to particle velocity, estimated from the peak-to-peak time of I_{Δ} (see Ref. [30] of the main text), and averaging over sixty particles ($7 \mu\text{m}$ diameter beads). It is pointed out that our observation model is obtained by purely electric measurements. The EKF has been implemented in a custom Matlab script, following Brazey et al. for the definition of the state model and of the covariances of measurement noise and disturbances. As a proof of concept, an example of EKF-based estimation of the longitudinal position of a flowing bead is shown in Figure S8(b).

As a perspective, integrating the approach for cross-sectional position sensing proposed in this work with the approach for longitudinal position sensing proposed by Brazey et al., our device could be optimized to provide fast and accurate 3D particle tracking.

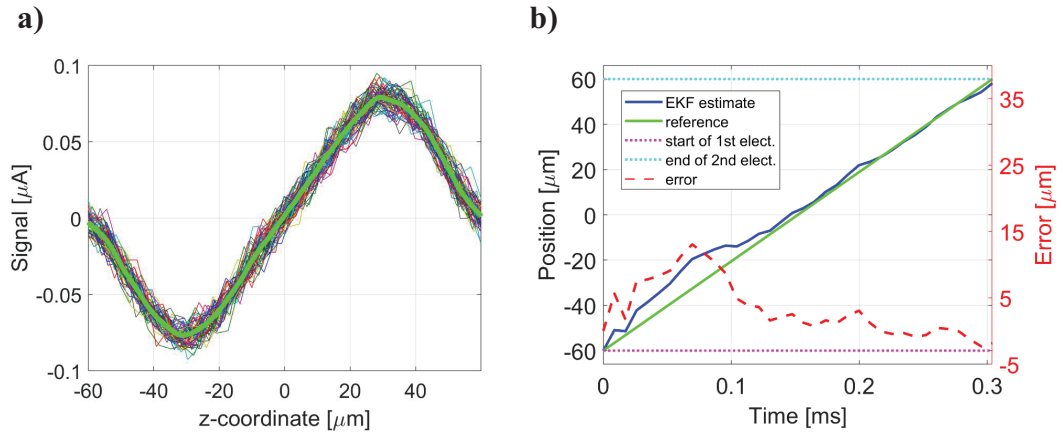


Figure S8: (a) Signal I_{Δ} as a function of the longitudinal particle position. Sixty traces are considered and the observation model (green thick line) is obtained by averaging. (b) Example of EKF-based estimation of longitudinal particle position (initial state vector $[-60 \mu\text{m}, 1.3v]$, where v is the true particle velocity). The true position is reported as reference, along with the relevant estimation error. The positions corresponding to the start of the first electrode pair and the end of the second electrode pair are also indicated.

9 Beads electrical volume

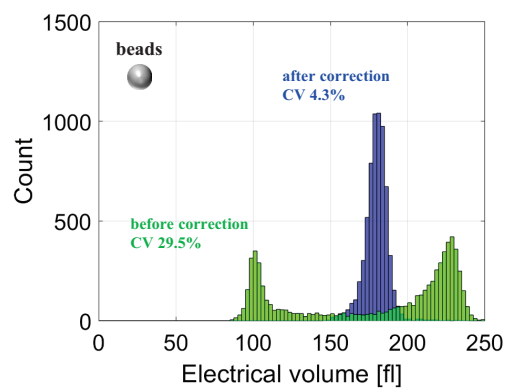


Figure S9: Histograms of the electrical volume of the beads before (in green) and after (in blue) the correction for positional-dependence (cf. Ref. [30] of the main text for full details on the compensation procedure).

10. Literature survey

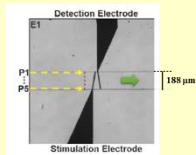
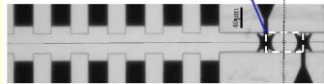
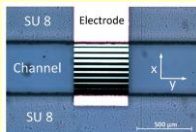
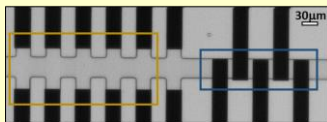
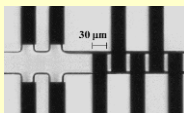
	Wang et al. <i>Lab Chip</i> 2017 [26]	Brazey et al. <i>Lab Chip</i> 2018 [27]	Solsona et al. <i>Lab Chip</i> 2019 [28]	Reale et al. <i>Microfluid. Nanofluid.</i> 2018 [29]	Present work
					
Demonstrated position detection along:	channel width	channel length	channel width	channel width and channel height (simultaneously)	channel width and channel height (simultaneously); potential for channel length
Experimental samples	6 and 11 μm diameter beads	8.7 μm diameter beads	83 μm diameter beads	6 and 10 μm diameter beads	human and chicken red blood cells (RBCs) spiked with 7 or 6 μm diameter beads
Channel dimensions (width x height)	188 μm x 17 μm	40 μm x 20 μm	477 μm x 219 μm	40 μm x 21.5 μm	50 μm x 21.5 μm
Technology	single pair of non-parallel surface microelectrodes	2 coplanar electrodes with non-classical shape + DEP-focusing electrode array	2 parallel (facing) electrode arrays	5 coplanar electrode pairs + 5 coplanar electrodes	2 coplanar electrode pairs + 5 coplanar electrodes
Principle	transit time through non-parallel electrodes	variation of impedance measured between two electrodes	gradient in electric field	ratio of transit times + relative prominence	peak unbalance + relative prominence
Number of acquired signals & relevant frequencies	1 signal @ 12 MHz	1 signal @ 500 kHz	1 signal @ (800 Hz & 100 kHz)	2 signals @ 1 MHz + 1 signal @ 885 kHz	1 signal @ 500 kHz + 1 signal @ (615 kHz & 1 MHz)
Accuracy in position detection	20% of channel width	<4 μm	12.5% of channel width	6% of channel width (lat. pos.); 8% of channel height (vert. pos.)	6% of channel width (lat. pos.); 8% of channel height (vert. pos.)
Demonstrated detection rate	up to 400 #/s	2 #/s (*)	0.3 #/s (*)	50-375 #/s (according to flow rate)	125-460 #/s (according to flow rate)
Statistical number	N/A	~10 exemplary events	<100 (*)	>2000	>2000
Demonstrated additional metrics for electrical particle/cell characterization	-	bead velocity	system conductivity	bead velocity	RBC/bead inter-arrival time; RBC/bead velocity profile (accuracy 5% of max velocity); bead volume (4.3% CV); RBC distribution width (RDW) and mean corpuscular volume (MCV); RBC/bead electrical opacity
Demonstrated application	discrimination of five different transverse bead positions	bead tracking, compatible with on-line processing	bead tracking and conductivity measurement	monitoring bead inertial focusing	monitoring RBC/bead hydrodynamic (sheath-flow) focusing

Table S4: Literature survey on recently proposed systems for electrical position detection (N/A: not available; (*): derived from data reported in the paper; lat.: lateral; vert.: vertical; pos.: position). Image snapshots from Refs. [26-28] of the main text are adapted with permission from The Royal Society of Chemistry.